Capsule of *Cryptococcus neoformans* grows by enlargement of polysaccharide molecules

Susana Frases[a], Bruno Pontes[b], Leonardo Nimrichter[c], Nathan B. Viana[b,d], Marcio L. Rodrigues[c], and Arturo Casadevall[a,e,1]

[a]Department of Microbiology and Immunology and [e]Division of Infectious Diseases of the Department of Medicine, Albert Einstein College of Medicine, 1300 Morris Park Ave, Bronx, NY 10461; [b]Laboratório de Pinças Óticas-Coordenação de Programas de Estudos Avançados, Instituto de Ciências Biomédicas, and [c]Laboratório de Estudos Integrados em Bioquímica Microbiana, Instituto de Microbiologia Professor Paulo de Góes,Universidade Federal do Rio de Janeiro, 21941-902, Rio de Janeiro, Brazil; and [d]Instituto de Física, Universidade Federal do Rio de Janeiro, 21941-972, Rio de Janeiro, Brazil

Edited by John B. Robbins, National Institutes of Health, Bethesda, MD, and approved December 1, 2008 (received for review September 10, 2008)

The human pathogenic fungus *Cryptococcus neoformans* has a distinctive polysaccharide (PS) capsule that enlarges during infection. The capsule is essential for virulence, but the mechanism for capsular growth is unknown. In the present study, we used dynamic light scattering (LS) analysis of capsular PS and optical tweezers (OT) to explore the architecture of the capsule. Analysis of capsular PS from cells with small and large capsules by dynamic LS revealed a linear correlation between PS effective diameter and microscopic capsular diameter. This result implied that capsule growth was achieved by the addition of molecules with larger effective diameter, such that some molecules can span the entire diameter of the capsule. Measurement of polystyrene bead penetration of *C. neoformans* capsules by using OT techniques revealed that the outer regions were penetrable, but not the inner regions. Our results provide a mechanism for capsular enlargement based on the axial lengthening of PS molecules and suggest a model for the architecture of a eukaryotic microbial capsule.

GXM | GalXM

Cryptococcus neoformans is an opportunistic fungal pathogen that causes meningoencephalitis, particularly in immunocompromised patients. The fungus is unique among human eukaryotic pathogens in that it has a polysaccharide (PS) capsule that is the major determinant of virulence (1). The capsule is composed of 2 major PS, galactoxylomannan (GalXM) and glucuronoxylomannan (GXM). GalXM is an α(1, 6)-galactan containing β(1, 3)oligosaccharyl substitutions at alternate residues of galactose. The oligosaccharide constituents of GalXM are trisaccharide motifs composed of α(1, 3)-mannosyl dimers in α (1, 4) linkages to galatosyl units. Each of the trisaccharide components may be substituted with β(1, 2)- or β(1, 3)-glucuronyl residues. GXM consists of a α-(1, 3)-mannan main chain with β(1, 2)-glucuronic acid residues attached to every third mannose, on average. Mannosyl residues can also be 6-*O*-acetylated and substituted with xylosyl units in β(1, 2)- or β(1, 4)-linkages (2). GXM and GalXM are released into culture media by growing cells as exo-PS that can be recovered for physical and chemical analysis. When coupled to protein, GXM can elicit protective antibodies (3).

C. neoformans cells increase their capsular diameter in response to diverse stressors, including mammalian infection (4). Capsule enlargement has been associated with virulence (5–8), and it protects the fungus against host defense mechanisms, such as phagocytosis and oxidative burst (9, 10). Although the biological properties of the capsule have been extensively studied, its architecture and mechanism of enlargement have not been fully elucidated. Capsule enlargement can occur by apical growth (7), and there is evidence that capsule size is regulated at the level of individual PS molecules (11). Given that GXM is a macromolecule, and that capsular assembly involves the noncovalent attachment of PS fibrils to the cell wall (12), and to each other (13, 14), it is likely that many aspects of capsule construction are directly related to the physical-chemical properties of the PS molecules. For example, there is evidence that capsular assembly is partly the result of inherent PS properties that promote self-assembly (14). Despite the extensive studies carried

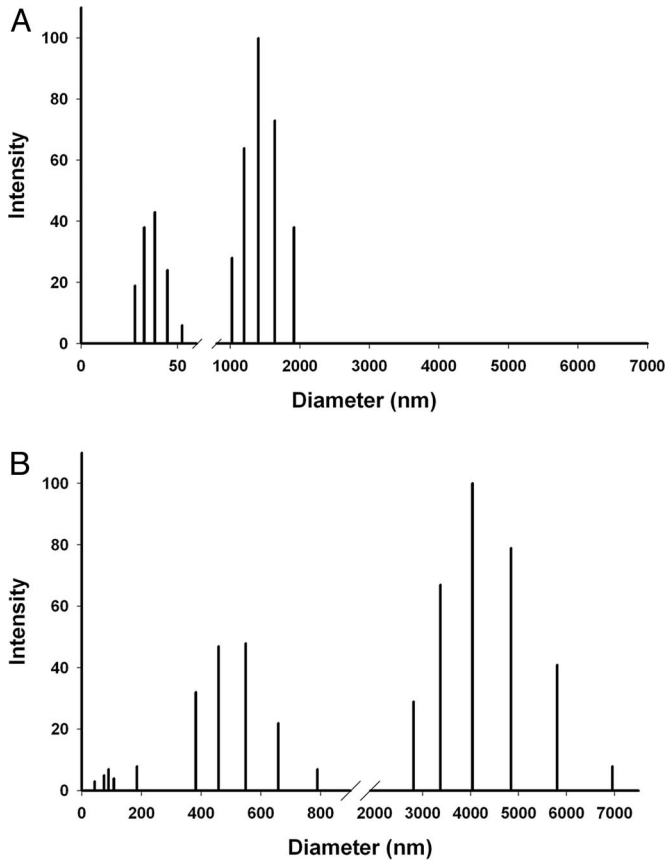

Fig. 1. Multimodal size distribution analysis of PS fractions; exo-PS (*A*) and capsular-PS (*B*) obtained from strain 24067 (serotype D). The *x* axis represents size distribution by particle diameter; *y* axis corresponds to the values of percentage intensity weighted sizes obtained from the NNLS algorithm (27).

Author contributions: S.F., L.N., N.B.V., M.L.R., and A.C. designed research; S.F. and B.P. performed research; S.F., B.P., L.N., N.B.V., M.L.R., and A.C. analyzed data; and S.F. wrote the paper.

The authors declare no conflict of interest.

This article is a PNAS Direct Submission.

[1]To whom correspondence should be addressed. E-mail: casadeva@aecom.yu.edu.

This article contains supporting information online at www.pnas.org/cgi/content/full/0808995106/DCSupplemental.

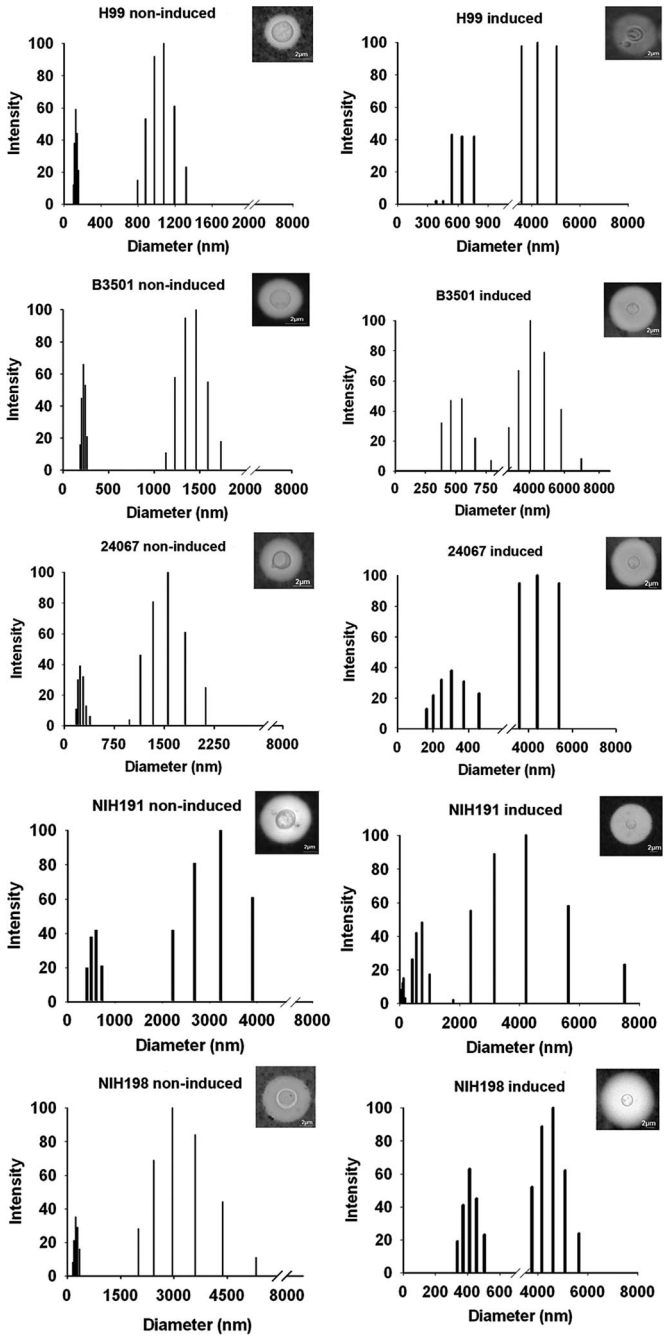

Fig. 2. Multimodal size distribution analysis of capsular-PS from strains H99, B3501, 24067 (*C. neoformans*), NIH191, and NIH198 (*C. gattii*) in noninducing and inducing media. The *x* axis represents particles size distribution measured as a diameter in nanometers; *y* axis corresponds to the values of percentage intensity weighted sizes obtained from the NNLS algorithm (27). (Scale bars, 2 μm.)

out with GXM, our information about *C. neoformans* capsular PS originates largely from studies of exo-PS components released from cells and recovered from culture supernatants. However, recent physical studies have shown significant differences between capsular PS and exo-PS, suggesting that these pools represent 2 different biosynthetic products (15). We applied dynamic light scattering (LS) to analyze the dimensions of PS molecules and optical tweezers (OT) to probe the strength of the capsule as a function of radius, and propose a model for capsule growth determined by molecular diameter.

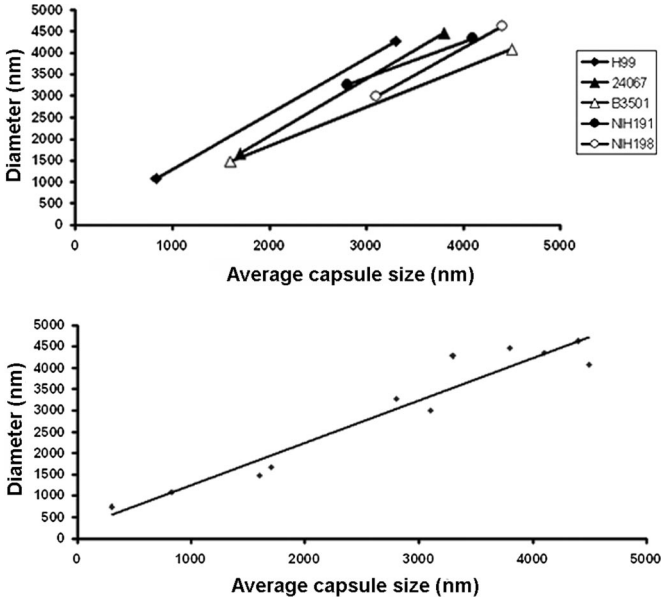

Fig. 3. Relationship between capsule size and effective diameter. Correlation between capsule size and PS fragments in *Cryptococcus* (*Upper*). Linear regression curve fitting ($Y = 0.9884x + 267.48$, $R^2 = 0.9297$) obtained from the average of capsular PS size measured by India ink negative stain and multimodal size distribution analysis of capsular PS from strains H99, B3501, 24067, 191, and 198 incubated in noninducing or capsule-inducing media. The *x* axis represents particles size distribution measured by India ink; *y* axis corresponds with average size values to the highest intensity weighted sizes obtained from the NNLS algorithm (27) (*Lower*).

Results

Effective Diameter and Polydispersity of Exo- and Capsular-PS. *C. neoformans* sheds large amounts of PS into culture media and infected tissues. To gain additional insight into the structural relationship between exo-PS and capsular PS, we determined average effective diameters and size distributions of PS from different samples by using quasy-elastic (QE)LS. Although both PS forms comprised PS of various diameters, capsular-PS had a significantly higher effective diameter than exo-PS [see Fig. 1 and supporting information (SI) Table S1]. The polydispersity of PS preparations was highest for exo-PS, suggesting that this material is more heterogeneous than capsular PS (Table S1).

Multimodal Size Distribution Analysis of Capsular-PS from 5 Cryptococcal Strains. Five strains were grown in noninducing and capsule-inducing conditions. PS was extracted and analyzed by QELS. For each strain, the capsular PS consisted of 2 populations, and induction of capsule size was associated with an increase in PS effective diameter (see Fig. 2 and Table S2). A plot of average capsule diameter obtained from India ink measurements versus the diameter of PS fragments revealed a linear correlation close to unity ($R^2 = 0.9297$; $P = 0.0386$) (Fig. 3). PS polydispersity values showed a broad range indicating significant heterogeneity for PS molecules in the samples.

Analysis of PS Fragments in Capsule Growth. Given that the correlation of effective diameter with capsular diameter implied a linear relationship, we sought to obtain additional evidence by analyzing the size of PS molecules during capsule growth as a function of time. A culture of *C. neoformans* was incubated for 120 h in conditions that promoted capsular enlargement. Every 24 h, an aliquot of cells was removed from the culture, and the capsular PS was extracted by DMSO, dialyzed against water, and then analyzed by QELS and multimodal size distribution anal-

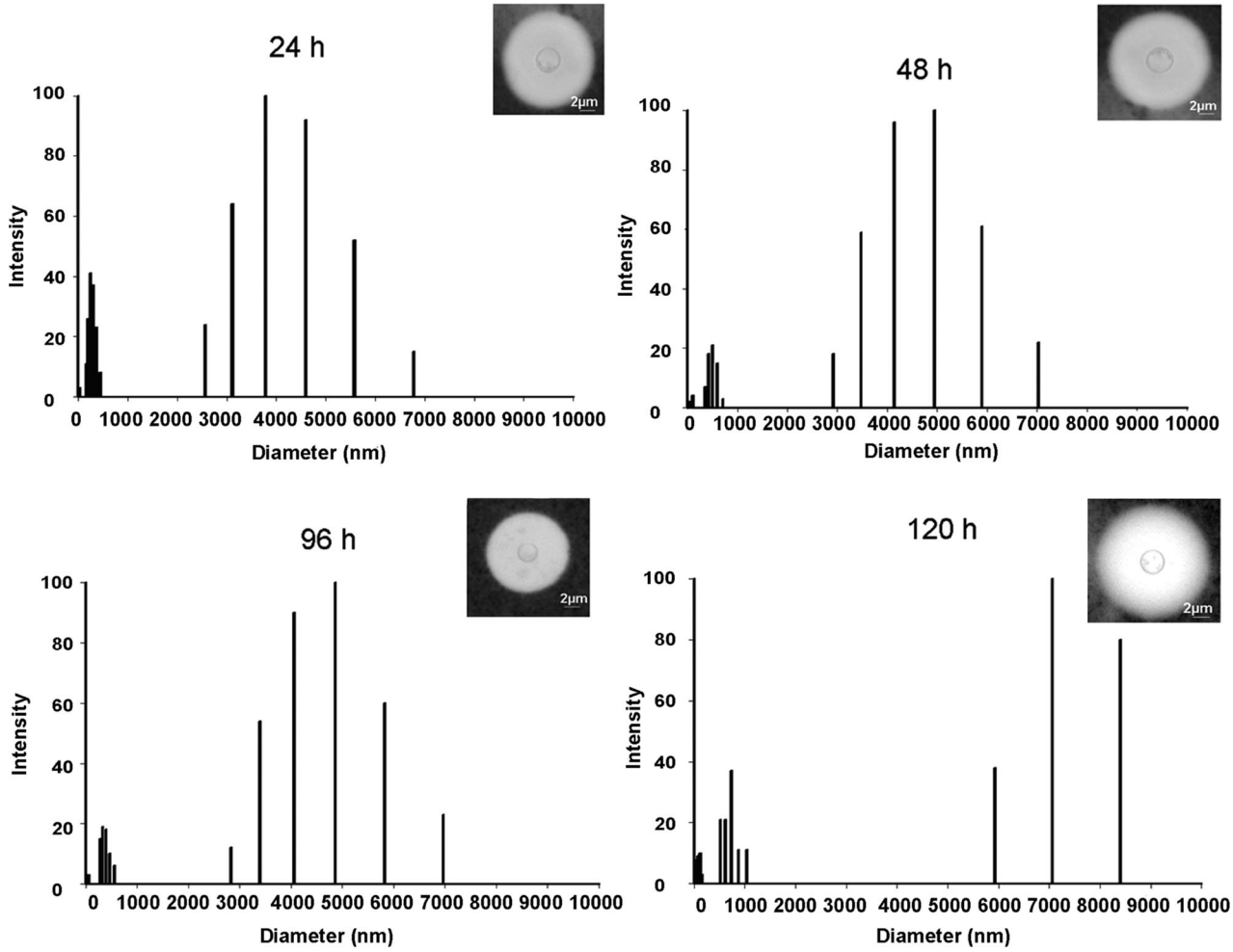

Fig. 4. Multimodal size distribution analysis of capsular-PS from *C. neoformans* (strain H99) in capsule-inducing media at different time points. The *x* axis represents particles size distribution measured as a diameter in nanometers; *y* axis corresponds to the values of percentage intensity weighted sizes obtained from the NNLS algorithm (27). (Scale bars, 2 μm.)

ysis. PSs from the cultures at time 0 showed 2 different size populations (50–200 and 500–1,200 nm) with the highest values at 150 and 658 nm, respectively. Two different populations in PS size were present at each time with the larger population progressively increasing in size over the time evaluated (Fig. 4 and Table S3), consistent with capsular enlargement occurring by the addition of molecules with greater diameter to the capsule.

Model of capsule architecture. By using the results of this study, prior contributions from several laboratories (4, 11, 16–18), and recent findings on the role of divalent cations on capsule structure (14), we propose a model for the architecture of the capsule (Fig. 5). Given that the most prevalent PS molecules are approximately of the same effective diameter as the capsule microscopic diameter, we propose that long molecules span the diameter of the capsule and serve as scaffolds for smaller molecules. Because the density of the capsule is greatest in the inner regions of the capsule (16, 19, 20), we propose that it is assembled by noncovalent binding of the smaller molecules to the larger molecules through interactions that include divalent cation bridges (Fig. 5). In this model, the small population of fibrils with effective diameters that exceed the capsule diameter measured with India Ink protrudes outside the India ink exclusion zone, and may be responsible for the fuzzy capsular edge apparent in India ink preparations. Hence, we propose that the architecture of the *C. neoformans* capsule consists of at least 3 zones that are defined by their relative PS density. Zone I is densest, closest to the cell body, and composed of a tight network of PS molecules. Zone II is an intermediate density zone that has sufficient mass to exclude India ink particles; however, it retains considerable permeability to macromolecules such as dextrans (16). Zone III has the lowest density and cannot exclude India ink particles; however, its presence can be gleaned by the fuzzy edges of some capsules.

Model Testing by Bead Penetration. The model proposed takes into account the observation that the *C. neoformans* capsule PS fibril density varies as a function of radial position (16). To obtain more experimental support for this model we studied the penetration of the PS capsule of *C. neoformans* by polystyrene beads by using OT. We captured a polystyrene sphere (a = 1.52 ± 0.02 μm) with the OT and pressed it against the capsule with a force of ≈400 pN (21) for 1 min to press the sphere to the fungus capsule. The results show that when the PS capsule is small, as happens in the early stages of growth, the beads can be pushed very closely to the cell wall (Fig. 6*A*). However, beads were not able to penetrate the inner portions of large capsules due to its high density (Fig. 6 *B* and *C*). These findings led us to define the zone I length by the distance between the cell wall and the bead (Fig. 6*D*). As the capsular enlarged, zone I also

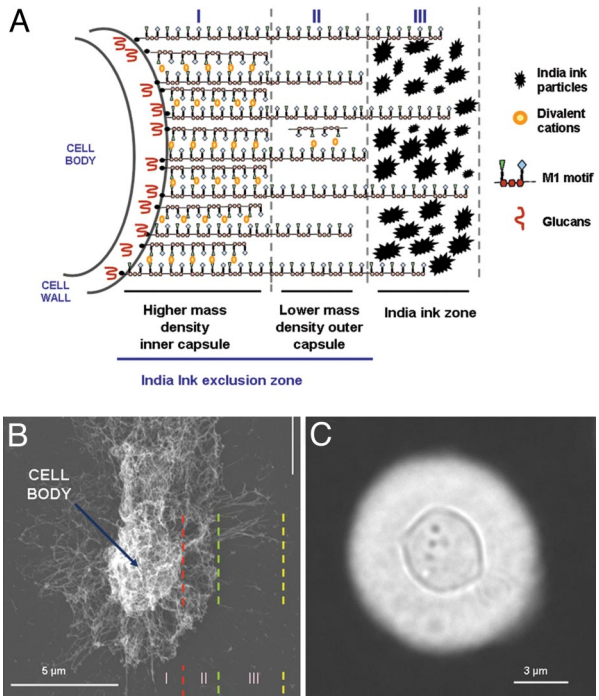

Fig. 5. Proposed model for *Cryptococcus neoformans* architecture. Capsule assemblage model (*A*). We provide a schematic representation that incorporates several observations made in this study and in recent reports from various laboratories, including ours (14, 16, 19, 28). GXM fibers are attached to cell wall glucans through noncovalent interactions (12, 28). To account for the observation that capsular PS density decreases as a function of radial distance (16, 19), we propose that the 2 major populations of GXM molecules such that the larger ones span the length of the India ink visible capsule and serve as a scaffold for the attachment of smaller fibrils. GXM-GXM interactions are thought to be mediated by the formation of divalent cation bridges (14). A small population of very large fibrils serves to extend the effective diameter of the capsule past the zone of India ink exclusion. Although the diagram shows GXM-GXM interactions limited to the inner layer only, we surmise that this interaction can occur throughout the capsule diameter with the caveat that they are more frequent in the inner layers of the capsule where they account for the higher density of those regions. Also, we have drawn the PS fibrils as linear molecules for simplicity, fully aware of the important caveat that scanning electron microscopy reveals that such molecules are tangled with apparent branching (13), and that such molecules have significant secondary structure (25). (*B*) Scanning electron microscopic image of a *C. neoformans* cell where zones I and II of the capsule are apparent by the density of fibrils. (*C*) *C. neoformans* cell suspended in India Ink. According to the model proposed in *A*, zone II ends at the exclusion boundary of India Ink particles. There is a fuzzy edge to the capsule, which we represent as occurring within zone III.

increased with time in agreement with the proposed model for capsular growth (Fig. 6*E*).

Discussion

Many types of pathogenic microbes have PS capsules that are essential for virulence. Despite their importance in microbial pathogenesis, capsules remain poorly understood. In comparison with the cell wall, capsular structures are fragile and easily disrupted by drying or radiation (20), making difficult the study of their physical properties. Cryptococcal capsular enlargement results in cells with diameter up to 50 μm that cannot be ingested by phagocytic cells (1). The capsule can enlarge by apical growth, but the mechanism responsible for spherical growth is unknown (7, 22). In this study we investigated the dimensions of capsular PS molecules in solution by dynamic LS to investigate the relationship between capsular diameter and molecular size.

Our study revealed that capsular PS molecules from diverse strains existed in 2 populations that differed in their effective diameter. Effective (or average) diameter is calculated from the LS data as the diameter of a theoretical molecule that has the same diffusion coefficient of the molecule being analyzed (23), and for a molecule like a PS, it is a measure of its hydrodynamic dimensions in solution. The most prevalent capsular PS effective diameters measured closely matched, or exceeded, the capsular diameter measured by India ink. This result implies that some PS molecules can span the entire length of the capsule. We also note that a small population of PS molecules was $\approx$7 μm in most of the strains studied, which is larger than the capsular diameter measured with India ink, suggesting extension of the capsule past the region of India ink exclusion.

Previously, we had suggested that a single molecule could not span the diameter of the capsule from studies of shed PS on the basis of radius of gyration (Rg) measurements from Zimm plots (13). However, that conclusion was based on studies of the PS released into the medium, which is significantly smaller than the capsular PS mass and effective diameter (15). Also, those measurements represented the average of all molecules in solution, and given the presence of discrete populations of different diameter described here, such averages would tend to significantly underestimate molecular dimensions.

Plots of effective diameter of capsular PS measured by QELS versus microscopic capsule size measurements revealed a linear correlation, strongly suggesting that capsule size is directly determined by PS molecule axial length. This observation is consistent with a recent study of shed exo-PS by gel electrophoresis, which suggested that capsule size is regulated at the polymer level (11), with the caveat that our study used capsular PS, which is considerably different from exo-PS (15). LS techniques also revealed the presence of PS molecules with smaller effective diameter that are presumably constituents of the capsule. To more firmly establish a relationship between PS effective diameter and capsule enlargement, we measured the distribution of fragments as a function of time for cells placed in capsular enlargement medium. Capsule enlargement was associated with an increase in PS effective diameter, resulting in the replacement of the shorter molecules with much longer molecules that closely approximated the capsule. A model of capsule growth whereby longer molecules are added to the capsule, and the older PS is retained near the cell wall would be consistent with our prior observation of capsular enlargement by apical growth (7).

PS molecules in all preparations existed in relatively narrow effective diameter populations. Size homogeneity implies tight control in the length polymerization of PS molecules, suggesting the existence of synthetic mechanisms that yield relatively uniform populations with discrete lengths. Consistent with the notion of different synthetic pathways for capsular PS and exo-PS, the latter accumulate in culture in late stationary phase without a significant reduction in capsule size. The finding that exo-PSs are different from capsular PSs may explain the inability to experimentally regenerate a normal capsule in acapsular mutants by the addition of exo-PS despite the fact that soluble PS does bind to the surface of acapsular strains (24) .

The application of QELS and molecular tweezers represents a previously undescribed approach to decipher the architecture of microbial PS capsules. Our findings support a model for the architecture of a microbial capsule whereby molecular length defines microscopic capsular diameter. However, the same findings pose several scientific questions that remain unstudied, including the identification of the mechanisms responsible for the relatively homogenous enlargement of PS molecules and the assembly of such large molecules into a spherical capsule. The *C. neoformans* capsule remains an enigmatic structure, but we are

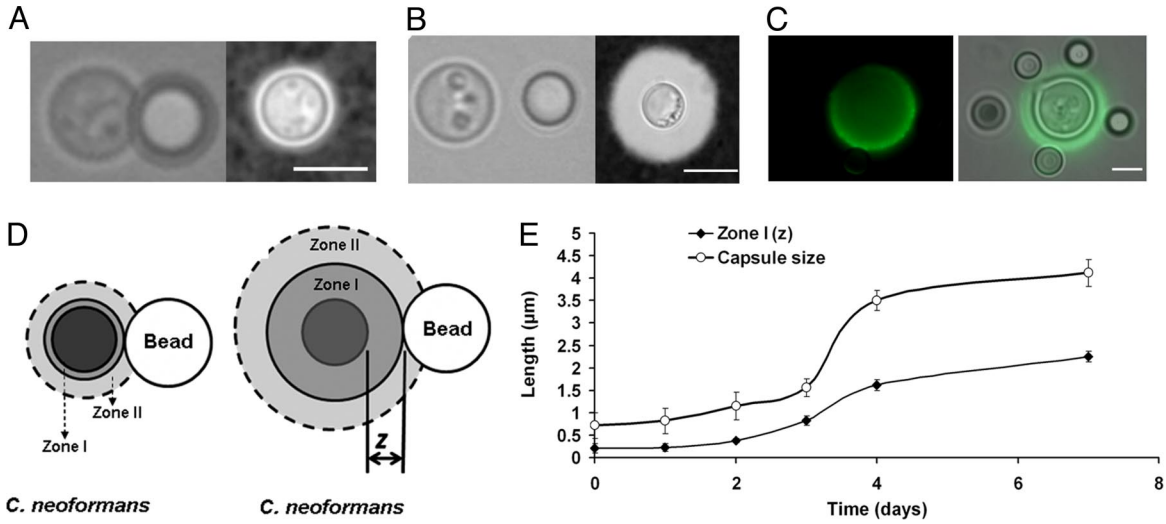

Fig. 6. Penetration of PS capsule by polystyrene bead. (*A*) Early stage in capsule growth showing a cell with a small capsule, confirmed by India ink negative stain and the bead adjacent to the cell wall. (*B*) Later stages in capsule growth showing a *C. neoformans* with a large capsule and the bead distant from the cell wall, represented by measured distance (z). (*C*) Imunofluorescence staining of capsular PS confirming that the beads penetrate the capsule (zone II), but do not touch the cell wall. (*D*) Schematic representation of measurements in which a is the radius of the bead and z is the zone I length in *C. neoformans*. (*E*) Filled circles, plot of the z during time; open circles, capsule size measurements by India ink stain. The *x* axis represents time point in days and *y* axis the length in micrometers. (Scale bars *A*–*C*, 3 μm.)

hopeful that its secrets will continue to yield to studies that combine approaches from multiple disciplines.

Experimental Procedures

***C. neoformans* Cultures.** The *C. neoformans* strains (ATCC 24067, H99, and B3501) and *Cryptococcus gattii* (NIH191 and NIH198) were grown in a minimal medium composed of glucose (15 mM), $MgSO_4$ (10 mM), KH_2PO_4 (29.4 mM), glycine (13 mM), and thiamine-HCl (3 μM); pH 5.5. Fungal cells were cultivated for 7 days at 30 °C. To induce capsule growth, the cells were transferred to PBS buffer with 10% FBS.

Isolation of Exo-PS from Culture Supernatants by Filtration. PS from 24067 cells was isolated by filtration and ultrafiltration, as described recently (14). Briefly, *C. neoformans* cells were separated from culture supernatants by centrifugation, and the resulting supernatant was concentrated ≈20-fold by using an Amicon (Millipore) ultrafiltration cell (cutoff, 100 kDa; total capacity of 200 mL) with stirring and Biomax polyethersulfone ultrafiltration discs (76 mm Millipore). After formation of a viscous film over the filtering disk, the fluid phase was discarded, and the remaining jellified material was recovered with a cell scrapper. The final PS solution was lyophilized and the dry PS mass determined.

Release of Capsular Components by Dimethyl Sulfoxide. Capsular PS was isolated as described (20). Yeast cells from all of the strains studied were washed 3 times in water. The cells were suspended in 15 mL of DMSO and incubated for 30 min. This process was repeated twice and the PS-containing fractions were combined. Cells were removed by centrifugation and the supernatant was then dialyzed against water for 12 h, with replacements by fresh water after 2-h intervals. The PS fractions were again dialyzed against water for 3 days.

PS Particle Sizes. The effective diameter and the polydispersity of PS preparations were measured by QELS in a 90Plus/BI-MAS Multi Angle Particle Sizing analyzer (Brookhaven Instruments). PS solutions were prepared as described above. The fluctuating signal, originating from the random motion of particles in a liquid phase and the associated alterations in the intensity of the scattered light over time, were processed by the autocorrelation function $C(t)$, $C(t) = Ae^{2\Gamma t} + B$. In this equation, t is the time delay, A is an optical constant determined by the instrument design, and Γ is related to the relaxation of the fluctuations by $\Gamma = Dq^2$. The value of q is calculated from the scattering angle θ, the wavelength of the laser light λ_0, and the index of refraction n of the suspended liquid, according to the equation $q = (2\pi n/\lambda_0)2\mathrm{Sin}(\theta/2)$. Particle size is related to the translational diffusion coefficient (D) as a function of molecular shape. Given scanning transmission micrographs showing PS molecules with and disordered branching pattern (13) and the observation that PS can have the same mass yet differ in Rg consistent with branching and/or significant secondary structure (25), we used the equation $D = (K_BT)/(3\pi\eta(t)d)$ for a branched polymer form, where K_B is Boltzmann's constant (1.38054×10^{-16} erg/K), T is the temperature in K (30 °C), $\eta(t)$ is the viscosity of the liquid in which the particles are moving, and d is the particle diameter. Polydispersity was defined as equal μ_2/Γ^2, where μ_2 is proportional to the variance of the intensity weighted distribution. The multimodal distributions of particle size diameter were generated by a nonnegatively constrained least squares algorithm (NNLS) based on the intensity of light scattered by each particle. For correlating the effective diameter of PS molecules with microscopic capsule diameter, we used QELS measurements with a cutoff of 80%, which represents the most prevalent PS population. All PS samples were analyzed under the same conditions.

Capsule Size Meassurments by India Ink Stain. Capsule size of 100 cells was measured in ImageJ 1.39u software [National Institutes of Health (NIH), Bethesda, MD]. Average and standard deviation were calculated.

Statistical Analysis. Statistical analyses were done with 90Plus/BI-MAS Software (Brookhaven Instruments).

Study of the Penetration of the Capsular PS by OT. OT, or optical trap, allow capture of small dielectric particles with diameters between ≈1 and 10 μm (26) to exert forces in the range of ≈1 to 500 pN (1 pN = 10 − 12N) (21). This property makes the OT a suitable instrument to measure events in a single cell experiment. The OT is a force sensor in the cellular force scale. The OT used in this work (21) is constructed by using an infra-red Nd:YAG laser with wavelength of 1.064 μm (Quantronix), a Gaussian intensity profile (TEM_{00} mode), and maximum power of 3 W. The laser beam intensity profile has a half-width of 2.3 ± 0.2 mm at the back focal plane of the objective lens as described (see ref. 21). The optical trap is constructed in an inverted Nikon Eclipse TE300 microscope, equipped with a PLAN APO 60 × 1.4 NA DIC H Nikon objective that is used to create the optical trap. Glass bottom dishes containing monoclonal antibody to GXM 18B7-coated glass coverslips were incubated with H99 *C. neoformans* cells in PBS for 1 h at room temperature. Then, polystyrene beads were added to the plate. To study the penetration of the bead into the PS capsule of *C. neoformans*, a polystyrene sphere (a = 1.52 ± 0.02 μm) was captured with the OT and then pressed against the capsule for 1 min to attach the sphere to the fungus capsule. The procedure was repeated 20 times for each time point (from day 0 to 7). Images were collected by a Hammamatsu C2400 CCD camera attached to the microscope. Measurements of bead penetration and intermediate zone length were done in ImageJ 1.39u software (NIH). Averages and SD were calculated.

Immunofluorescence was done by using 1×10^6 cells per mL. Cells were washed in PBS and blocked with PBS plus 1% BSA for 1 h at 37 °C. Then, they were incubated with 2 μg/mL anticapsular monoclonal antibody 18B7 for 1 h at 37 °C. After washing the excess of antibody with PBS, 10 μg/mL FITC-labeled IgG to murine Ig was added and incubated for another 1 h at 37 °C. Cells were washed with PBS and added to a plastic plate containing 18B7-coated glass coverslip. After 1-h incubation at room temperature, uncoated polystyrene beads were added to the plate. The plate was then placed in the microscope and an optical trap laser was used, as described before, to grab the beads in solution and place them in contact with the capsule. Images were taken in an inverted microscope (Eclipse TE300 Nikon) equipped with Plan APO 100 $\times$ 1.4 NA DIC H. Fluorescence images were taken by a Cool Snap Pro Color Roper Scientific CCD camera that digitizes them directly to the computer, and were captured employing ImagePro Plus (Media Cybernetics). Image analysis was performed with ImageJ (http://rsb.info.nih.gov/ij), and data analysis with Kaleidagraph (Synergy Software).

ACKNOWLEDGMENTS. We thank Allan J. Guimaraes, Johanna Rivera, Joshua Nosanchuk, and Vivaldo Moura Neto for discussions and assistance with various aspects of this work. A.C. and S.F. were supported by National Institutes of Health Awards AI033774, 5R01HL059842, and 2R37AI033142. M.L.R. and L.N. are supported by grants from the Brazilian agencies Conselho Nacional de Desenvolvimento Científico e Tecnológico (CNPq), Fundação de Amparo à Pesquisa do Estado do Rio de Janeiro (FAPERJ), and Fundação de Amparo à Pesquisa do Estado de São Paulo (FAPESP). N.B.V. and B.P. were supported by the Brazilian agencies CNPq, Fundação Coordenação Aperteiçoamento Avanço de Pessoal de Nível Superior, Instituto do Milênio de Nanociências, Instituto do Milênio de Avanço Global e Integrado da Matemática Brasileira, FAPERJ, and Fundação Universitária José Bonifácio.

1. Casadevall A, Perfect JR (1998) *Cryptococcus neoformans* (Am Soc Microbiol, Washington, DC).
2. Cherniak R, Valafar H, Morris LC, Valafar F (1998) Cryptococcus neoformans chemotyping by quantitative analysis of 1H nuclear magnetic resonance spectra of glucuronoxylomannans with a computer-simulated artificial neural network. *Clin Diagn Lab Immun* 5:146–159.
3. Devi SJ, *et al.* (1991) Cryptococcus neoformans serotype A glucuronoxylomannan-protein conjugate vaccines: Synthesis, characterization, and immunogenicity. *Infect Immun* 59:3700–3707.
4. Charlier C, *et al.* (2005) Capsule structure changes associated with Cryptococcus neoformans crossing of the blood-brain barrier. *Am J Pathol* 166:421–432.
5. Bulmer GS, Sans MD, Gunn CM (1967) *Cryptococcus neoformans* I. Nonencapsulated mutants. *J Bacteriol* 94:1475–1479.
6. Kozel TR, *et al.* (1988) Role of the capsule in phagocytosis of Cryptococcus neoformans. *Rev Infect Dis* 2:S436–439.
7. Zaragoza O, *et al.* (2006) The polysaccharide capsule of the pathogenic fungus Cryptococcus neoformans enlarges by distal growth and is rearranged during budding. *Mol Microbiol* 59:67–83.
8. D'Souza CA, *et al.* (2001) Cyclic AMP-dependent protein kinase controls virulence of the fungal pathogen Cryptococcus neoformans. *Mol Cell Biol* 21:3179–3191.
9. Zaragoza O, *et al.* (2008) Capsule enlargement in *Cryptococcus neoformans* confers resistance to oxidative stress suggesting a mechanism for intracellular survival. *Cell Microbiol* 10:2043–2057.
10. Zaragoza O, Taborda CP, Casadevall A (2003) The efficacy of complement-mediated phagocytosis of Cryptococcus neoformans is dependent on the location of C3 in the polysaccharide capsule and involves both direct and indirect C3-mediated interactions. *Eur J Immunol* 33:1957–1967.
11. Yoneda A, Doering TL (2008) Regulation of Cryptococcus neoformans capsule size is mediated at the polymer level. *Eukaryot Cell* 7:546–549.
12. Reese AJ, Doering TL (2003) Cell wall alpha-1,3-glucan is required to anchor the Cryptococcus neoformans capsule. *Mol Microbiol* 50:1401–1409.
13. McFadden DC, De Jesus M, Casadevall A (2006) The physical properties of the capsular polysaccharides from Cryptococcus neoformans suggest features for capsule construction. *J Biol Chem* 281:1868–1875.
14. Nimrichter L, *et al.* (2007) Self-Aggregation of Cryptococcus neoformans Capsular Glucuronoxylomannan Is Dependent on Divalent Cations. *Eukaryot Cell* 6:1400–1410.
15. Frases S, *et al.* (2008) Cryptococcus neoformans capsular polysaccharide and exopolysaccharide fractions manifest physical, chemical, and antigenic differences. *Eukaryot Cell* 7:319–327.
16. Gates MA, Thorkildson P, Kozel TR (2004) Molecular architecture of the Cryptococcus neoformans capsule. *Mol Microbiol* 52:13–24.
17. Pierini LM, Doering TL (2001) Spatial and temporal sequence of capsule construction in Cryptococcus neoformans. *Mol Microbiol* 41:105–115.
18. Janbon G (2004) Cryptococcus neoformans capsule biosynthesis and regulation. *FEMS Yeast Res* 4:765–771.
19. Maxson ME, Dadachova E, Casadevall A, Zaragoza O (2007) Radial mass density, charge, and epitope distribution in the Cryptococcus neoformans capsule. *Eukaryot Cell* 6:95–109.
20. Bryan RA, *et al.* (2005) Radiological studies reveal radial differences in the architecture of the polysaccharide capsule of Cryptococcus neoformans. *Eukaryot Cell* 4:465–475.
21. Viana NB, *et al.* (2007) Towards absolute calibration of optical tweezers. *Phys Rev* 75:021914.
22. McFadden D, Zaragoza O, Casadevall A (2006) The capsular dynamics of Cryptococcus neoformans. *Trends Microbiol* 14:497–505.
23. Chylek P (1986) Absorption and scattering of light by small particles. By C. F Bohren and D. R. Huffman. *Appl Opt* 25:3166.
24. Kozel TR, Gotschlich EC (1982) The capsule of cryptococcus neoformans passively inhibits phagocytosis of the yeast by macrophages. *J Immunol* 129:1675–1680.
25. McFadden DC, Fries BC, Wang F, Casadevall A (2007) Capsule structural heterogeneity and antigenic variation in Cryptococcus neoformans. *Eukaryot Cell* 6:1464–1473.
26. Ashkin A, Dziedzic JM, Yamane T (1987) Optical trapping and manipulation of single cells using infrared laser beams. *Nature* 330:769–771.
27. Lawson CL, Hanson RJ (1974) *Solving Least Squares Problems* (Prentice-Hall, Englewood Cliffs, NJ).
28. James PG, *et al.* (1990) Cell-wall glucans of Cryptococcus neoformans Cap 67. *Carbohydr Res* 198:23–38.